

1 **Mutually opposing activity of PIN7 splicing isoforms is required**
2 **for auxin-mediated tropic responses in *Arabidopsis thaliana***

3

4 **Ivan Kashkan^{1,2}, Mónica Hrtyan², Roberta Filepová¹, Zuzana Vondráková¹, Jan**
5 **Hejátko², Sibú Simon¹, Debbie Rombaut^{3,4}, Thomas B. Jacobs^{3,4}, Mikko J. Frilander⁵,**
6 **Jiří Friml⁶, Jan Petrášek¹, Kamil Růžička^{1,2,7,*}**

7

8 ¹*Laboratory of Hormonal Regulations in Plants, Institute of Experimental Botany, Czech Academy of*
9 *Sciences, 16502 Prague, Czech Republic*

10 ²*Functional Genomics and Proteomics of Plants, Central European Institute of Technology and*
11 *National Centre for Biomolecular Research, Masaryk University, 62500 Brno, Czech Republic*

12 ³*Department of Plant Biotechnology and Bioinformatics, Ghent University, 9052 Ghent, Belgium*

13 ⁴*VIB Center for Plant Systems Biology, 9052 Ghent, Belgium*

14 ⁵*Institute of Biotechnology, University of Helsinki, 00014 University of Helsinki, Finland*

15 ⁶*Institute of Science and Technology (IST Austria), 3400 Klosterneuburg, Austria*

16 ⁷*Lead Contact*

17

18 *Correspondence: kamil.ruzicka@ueb.cas.cz

19

20 **SUMMARY**

21 Advanced transcriptome sequencing has revealed that the majority of eukaryotic genes
22 undergo alternative splicing (AS). Nonetheless, limited effort has been dedicated to
23 investigating the functional relevance of particular splicing events, even those in the key
24 developmental and hormonal regulators. Here we reveal, in the plant model *Arabidopsis*
25 *thaliana*, that the *PIN7* gene, which encodes a polarly localized transporter for the
26 phytohormone auxin, produces two evolutionarily conserved transcripts. These isoforms
27 *PIN7a* and *PIN7b*, differing in a 4 amino acid motif, are present at nearly equal levels in most
28 cells, except some early developing tissues where the expression of *PIN7b* is moderately
29 prevalent. Both proteins also transport auxin with similar capacity and directionality.
30 However, only *PIN7a* but not *PIN7b* cDNA rescues the phenotypes associated with the *pin7*
31 knock-out mutation, consistent with their differences in the subcellular trafficking and
32 dynamics at the plasma membrane. Further phenotypic analyses suggested a joint, mutually
33 opposing activity of both isoforms as being required for correct seedling apical hook
34 formation and auxin-mediated tropic responses. These results establish alternative splicing of
35 the PIN family as an evolutionary conserved, functionally relevant mechanism, taking part in
36 the auxin-mediated plant development.

37

38 **KEYWORDS**

39 Auxin, auxin transport, PINs, alternative splicing, plant development, RNA processing, tropic
40 responses

41

42 **INTRODUCTION**

43 Auxin is an essential phytohormone, which plays a role in nearly all aspects of plant
44 development. To flexibly adapt to rapidly changing environmental cues, directional auxin
45 transport represents a highly dynamic means for triggering downstream morphogenetic
46 processes. PIN FORMED (PIN) auxin efflux carriers are among the key regulators in this
47 respect. Many efforts in the past years uncovered several mechanisms operating
48 transcriptionally or post-translationally on the capacity and directionality of PIN-mediated
49 transport. However, little progress has been made in exploring the contribution of post-
50 transcriptional regulation (Adamowski and Friml, 2015; Hrtyan et al., 2015).

51 Advances in high throughput sequencing have revealed unexpected complexity within
52 eukaryotic transcriptomes by alternative splicing (AS). Although the majority of AS
53 transcripts may be functionally neutral (Darracq and Adams, 2013; Reddy et al., 2013; Tress

54 et al., 2017; Blencowe, 2017; Mei et al., 2017), several detailed studies have highlighted a
55 plausible role for numerous AS events in physiologically relevant contexts, including those
56 involved in plant developmental and hormonal pathways (Staiger and Brown, 2013; Hrtyan et
57 al., 2015; Shang et al., 2017; Szakonyi and Duque, 2018). Earlier works have described
58 auxin-related defects resulting from the aberrant function of several regulators of AS (Kalyna
59 et al., 2003; Casson et al., 2009; Retzer et al., 2014; Tsugeki et al., 2015; Hrtyan et al., 2015;
60 Bazin et al., 2018). AS changes subcellular localization of the auxin biosynthetic gene
61 *YUCCA 4* (Kriechbaumer et al., 2012) and differential splicing of an exon (Marquez et al.,
62 2015) inside the *AUXIN RESPONSE FACTOR 8* results in developmental changes of
63 generative organs (Ghelli et al., 2018). AS of the Major Facilitator Superfamily transporter
64 *ZIFL1* interferes with auxin transport, influencing the stability of PINs on the plasma
65 membrane (PM) (Remy et al., 2013). These lines of evidence suggest that AS is an important
66 player in auxin-dependent processes. However, no coherent functional model of any auxin-
67 related AS event has been provided so far.

68 Here, we characterize AS of the *PIN7* gene in *Arabidopsis thaliana*. *PIN7* is, together
69 with *PIN3* and *PIN4*, a member of the *PIN3* clade of PIN auxin efflux carriers (Bennett et al.,
70 2014), which are required for a broad range of morphogenetic and tropic processes
71 (Adamowski and Friml, 2015). We reveal that AS influences the dynamics of the *PIN7*
72 protein on the PM. We also demonstrate that the coordinated action of both splice variants is
73 required for fine-tuning auxin-mediated tropic responses and during apical hook development.

74

75 RESULTS

76 *Arabidopsis PIN7* and *PIN4* produce two evolutionarily conserved AS transcripts

77 Our previous survey (Hrtyan et al., 2015) revealed that several genes involved in
78 auxin-dependent processes undergo AS. Among them, closely related paralogs from the *PIN3*
79 clade of auxin transporters, *PIN4* and *PIN7* (but not *PIN3*), are regulated by the same type of
80 AS (Petrasek et al., 2006; Bennett et al., 2014; Hrtyan et al., 2015). The resulting transcripts,
81 denoted as *a* and *b*, differ in the position of the AS donor site in the first intron (Figure 1A).
82 The differentially spliced region corresponds to a four amino acid motif inside the large
83 internal hydrophilic loop (Ganguly et al., 2014; Nodzyński et al., 2016) of the integral PM
84 transporter (Figure 1A and 1B). We examined the quantities of individual reads spanning the
85 exon junctions in the respective region from the *Arabidopsis* root tip and in several other
86 available transcriptomes from different tissues and organs (Klepikova et al., 2016; Cheng et
87 al., 2017; Ruzicka et al., 2017) (Figures 1C and Supplemental Figure 1A). We found that both

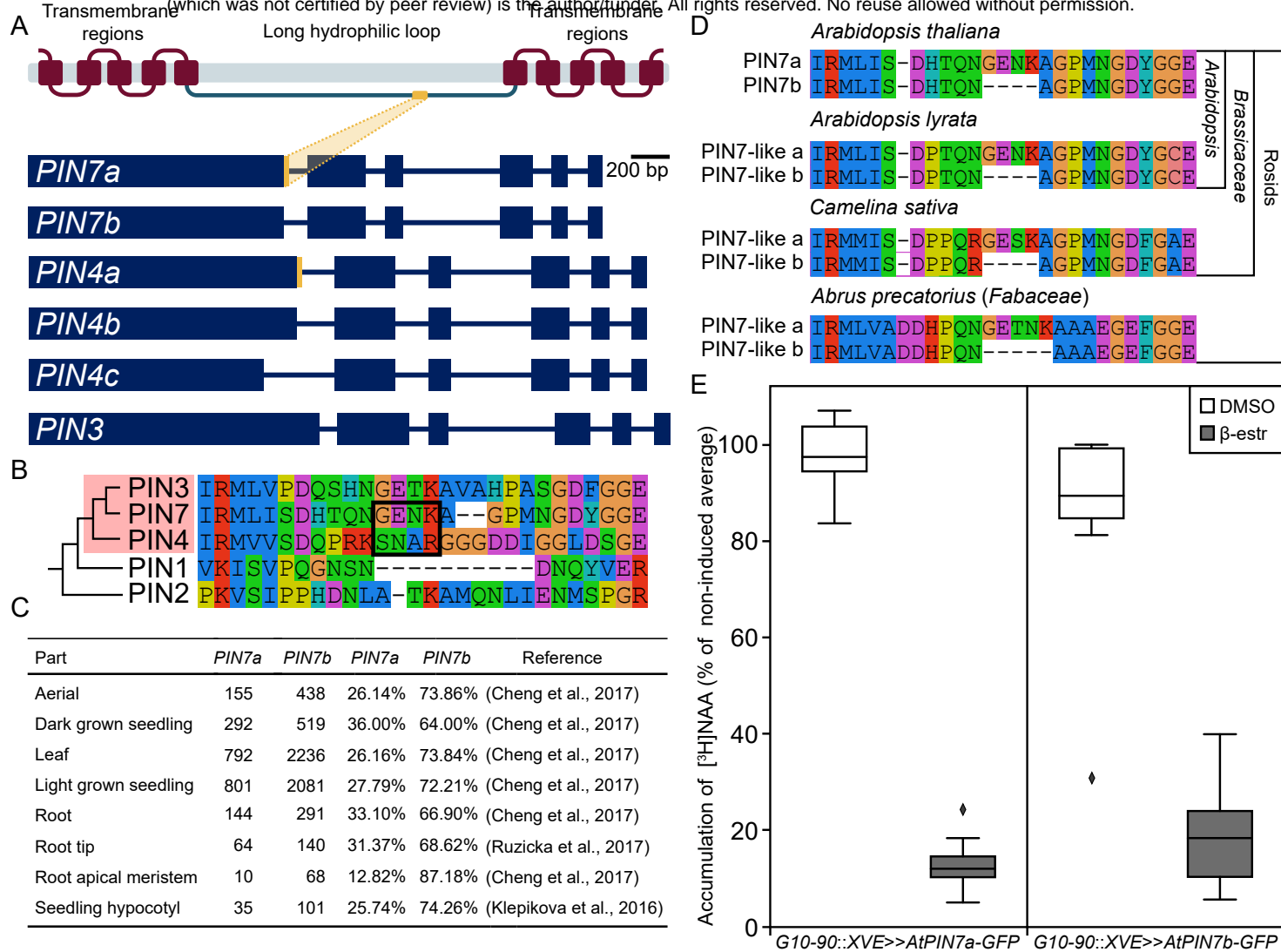


Figure 1. Alternative splicing (AS) of the Arabidopsis thaliana PIN7 and PIN4 leads to two evolutionary conserved functional transcripts.

(A) Scheme of coding regions of the PIN3 clade genes in Arabidopsis thaliana. The alternative donor splice site at the end of the first exon of PIN7 and PIN4, respectively, but not PIN3, results in two transcripts differing in 12 nucleotides. This sequence (orange) corresponds to the protein motif, located in the long internal hydrophilic loop of the transporter. There is also an additional PIN4c transcript present in publicly available transcriptomes.

(B) Amino acid alignment of the region around the 4-amino acid motif changed by AS in the PIN3 clade proteins (boxed in pink) in Arabidopsis thaliana, including the closest PIN paralogs.

(C) Table shows the number of RNA-seq reads spanning the exon1-exon2 junction corresponding to the detected PIN7 transcripts in selected Arabidopsis thaliana tissue sources. Their ratio was calculated as a percentage of total reads mapped to this area as assessed from the genome browser graphic interface.

(D) Protein sequence alignment showing the conservation of AS in the PIN3 clade of auxin transporters among rosids.

(E) Accumulation of [3H]NAA in BY-2 cells following induction of Arabidopsis thaliana G10-90::XVE>>AtPIN7a-GFP and G10-90::XVE>>AtPIN7b-GFP cDNAs with 1 μ M β -estradiol. [3H]NAA accumulations within the observed period show no difference between both tested isoforms. The values shown in box plots were normalized to the average maximum of the [3H]NAA accumulation rates in the non-induced lines. Middle line shows median, the box corresponds to the 25% and 75% quartiles, the whiskers represent minima and maxima (n = 9).

See also Supplemental Figure 1.

88 *PIN4*- and *PIN7a* and *b* transcripts are expressed abundantly in all tissues, independently on
89 the data set inspected. Besides these AS events, we also identified a minor *PIN4c* (Marquez et
90 al., 2012; Hrtyan et al., 2015) splice isoform (but not corresponding *PIN7c*), which comprised
91 around 3-7% of the *PIN4* exon1-exon2 spanning reads (Figures 1A and Supplemental Figure
92 1A). Other occasionally observed transcripts (also corresponding to the other exon junctions)
93 were not repetitively seen among different RNA-seq data sets. It thereby appears that *PIN7*
94 and *PIN4* are processed into two and three transcripts, respectively, and that *PIN7a* and *b* (or
95 *PIN4a* and *b*) are expressed in most of the plant organs at comparable or nearly similar levels.

96 Functionally relevant AS events are commonly evolutionarily conserved (Keren et al.,
97 2010; Reddy et al., 2013), therefore we sought for available validated transcripts to determine
98 whether similar splicing events occur in orthologous *PIN3* clade genes in other dicot species
99 (Bennett et al., 2014; O’Leary et al., 2016). We found examples of such mRNAs besides
100 members of the *Brassicaceae* family, for instance, also in *Abrus precatorius* (*Fabaceae*),
101 which documents the conservation of this AS event in rosids, a plant clade which diversified
102 more than 100 million years ago (Li et al., 2019) (Figure 1D). *PIN4c* did not show any deeper
103 evolutionary conservation. Thus, at least some genes of the *PIN3* clade are regulated by the
104 same type of AS, across several plant families, which suggests that these AS events may have
105 a relevant biological function.

106

107 ***PIN7a* and *PIN7b* transport auxin with comparable rates in tobacco cells**

108 To test whether both protein isoforms indeed function as auxin transporters, we
109 exemplified this on the expression of the *PIN7a* and *b* cDNA variants tagged with GFP,
110 respecting the design of the original *PIN7-GFP* construct (Blilou et al., 2005), under the
111 control of the β -estradiol-driven promoter in tobacco BY-2 cells (Petrasek et al., 2006; Müller
112 et al., 2019). Following induction of both transgenes, we observed a comparable decrease of
113 radioactive-labeled auxin accumulation inside the BY-2 cells (Figure 1E) and the time course
114 of the auxin accumulation drop appeared to be similar for both constructs (Supplemental
115 Figure 1B), in accord to that of *PIN7a* cDNA, examined previously (Petrasek et al., 2006).
116 These experiments reveal that *PIN7a* and *PIN7b* code for true auxin exporters, which
117 transport auxin at similar rates in tobacco cell cultures.

118

119 **AS changes subcellular dynamics of PIN proteins**

120 Polarity and dynamic intracellular trafficking are essential functional attributes of
121 PINs (Adamowski and Friml, 2015). We expressed fluorescently-tagged cDNA versions of

122 the respective *PIN7* and *PIN4* transcripts under their native promoters in *Arabidopsis*
123 *thaliana*. Their overall expression patterns resembled those of the *PIN7-GFP* and *PIN4-GFP*
124 lines made on the basis of the genomic sequence (Supplemental Figures 2A-2D). At the
125 cellular level, the protein isoform localization did not largely differ from each other in terms
126 of polarity or general subcellular localization in the root tip (Figure 2A). Thus, at a given
127 resolution, it appears that the motif substituted during AS does not change the basic
128 subcellular localization or expression pattern of both PIN7 and PIN4 proteins.

129 The anterograde trafficking of proteins towards PM can be effectively blocked by the
130 fungal toxin brefeldin A (BFA). It leads to internal accumulation of the membrane-bound
131 PINs into characteristic BFA bodies (Geldner et al., 2001; Kleine-Vehn et al., 2010). During
132 time-lapse imaging, we observed that while PIN7a-GFP accumulated readily in these
133 intracellular aggregates, PIN7b-RFP formed less pronounced aggregates, co-localizing with
134 PIN7a-GFP incompletely (Figures 2A and 2B; Supplemental Figure 2E). To exclude that the
135 fluorescent tag influences the sensitivity of the PIN7 intracellular trafficking caused by BFA,
136 we compared the response of PIN7a-GFP with additionally generated PIN7b-GFP cDNA
137 expressing lines. We observed that the BFA mediated aggregation of PIN7b-GFP indeed
138 showed a moderate delay, compared with PIN7a-GFP (Figure 2C). These observations
139 suggest that the PIN7 isoforms differ in the speed of their intracellular trafficking pathways or
140 delivery to the PM and the choice of the tag does not appear to interfere significantly with the
141 subcellular dynamics of PIN7.

142 PIN polarity does not seem to strictly require the cytoskeleton (Glanc et al., 2018), but
143 subcellular PIN trafficking has been proposed to be mediated by two distinct pathways
144 (Geldner et al., 2001; Glanc et al., 2018). The first is dependent on actin filaments
145 (cytochalasin D-sensitive) and occurs in most cells of the root meristem. The second
146 (oryzalin-sensitive) utilizes microtubules and is linked with cytokinesis. Drugs that
147 depolymerize actin filaments (cytochalasin D) and tubulin (oryzalin) (Geldner et al., 2001;
148 Kleine-Vehn et al., 2008b) showed only little effect on the intracellular localization of both
149 PIN7 isoforms when applied alone (Supplemental Figures 2F and S2G). Pretreatment with
150 cytochalasin D prevented the formation of the BFA bodies (Geldner et al., 2001) containing
151 both PIN7 isoforms (Figure 2D). Yet, when we applied oryzalin prior to the BFA treatment,
152 the BFA compartments containing PIN7a-GFP and PIN7b-RFP associated in only very
153 weakly co-localizing structures (Figure 2E).

154 Next, we tested how the cytoskeleton is involved in the trafficking of both PIN7
155 isoforms from the BFA bodies to the PM by washing out BFA with cytochalasin D or

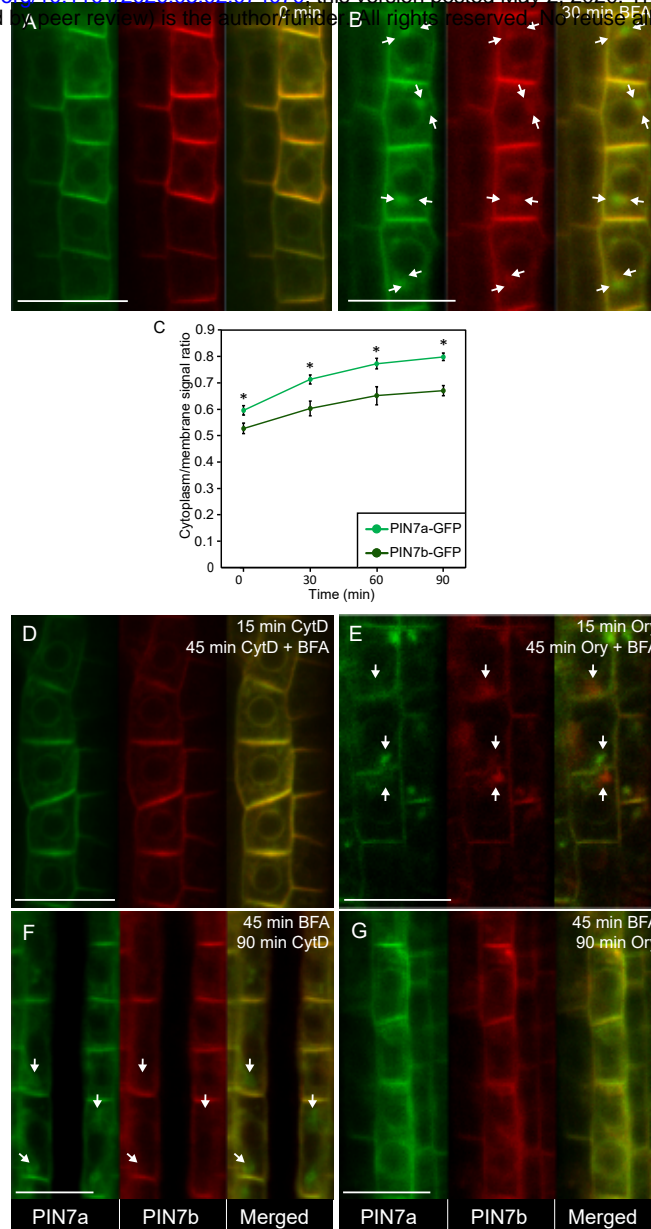


Figure 2. PIN7a-GFP and PIN7b-RFP cDNA-encoded proteins show similar cellular localization patterns but differ in response to brefeldin A (BFA) and the cytoskeletal drugs in the Arabidopsis primary root meristem.

(A) Subcellular localization and polarity of untreated PIN7a-GFP and PIN7b-RFP cDNA-encoded proteins in the primary root meristem cells.

(B) Both PIN7a-GFP and PIN7b-RFP aggregate in the intracellular compartments (BFA bodies) after 30 min of 50 μ M BFA treatment, but do not fully co-localize (arrows).

(C) Temporal dynamics of BFA mediated aggregation of PIN7a-GFP and PIN7b-GFP inside cells. The values were determined as a ratio of fluorescence intensities between the cytoplasm and plasma membrane. (* $P < 0.05$ by ANOVA, $n = 12$). Data are means \pm S. E.

(D) The fluorescence signal from PIN7a-GFP and PIN7b-RFP upon disruption of actin filaments with 20 μ M cytochalasin D for 15 min followed by the addition of 50 μ M BFA for another 45 min.

(E) PIN7a-GFP and PIN7b-RFP aggregation (arrows) upon disruption of microtubules with 20 μ M oryzalin for 15 min, followed by the addition of 50 μ M BFA for another 45 min.

(F) Effect of cytochalasin D on the PIN7a-GFP and PIN7b-RFP exit from the BFA bodies upon 45 min pre-treatment with 50 μ M BFA and followed by wash-out with 20 μ M cytochalasin D for another 90 min.

(G) Effect of oryzalin on the PIN7a-GFP and PIN7b-RFP exit from the BFA bodies upon 45 min pre-treatment with 50 μ M BFA and followed by wash-out 20 μ M oryzalin.

In (A, B and D-G), the signals of 3 cells in each of 5 root tips were analyzed ($n = 15$); bars, 10 μ m.

See also Supplemental Figure 2.

156 oryzalin (Geldner et al., 2001). In the presence of cytochalasin D, PIN7a-GFP largely
157 persisted inside the BFA bodies, while the PIN7b-RFP signal was almost absent in these
158 aggregates (Figure 2F). We generally did not see any difference between both isoforms when
159 BFA was washed out with oryzalin (Figure 2G). These data thereby suggest that both PIN7
160 isoforms use vesicle trafficking pathways that are assisted by a common cytoskeletal scaffold.
161 These pathways differ in their dynamics and the endomembrane components involved and are
162 consistent with previous findings that individual PINs can utilize multiple PM delivery routes
163 (Boutté et al., 2006; Kleine-Vehn et al., 2008b).

164

165 **AS affects dynamics of PIN7 at the PM but not its ability to relocate in response to** 166 **tropic stimuli**

167 Complementary to the observations obtained by the pharmacological approach, we
168 tracked intracellular PIN7 dynamics under natural conditions. Auxin transporters of the PIN3
169 clade change their polar localization on the PM by the reaction to various environmental cues,
170 in particular by switching the light or gravity vectors (Friml et al., 2002; Rakusová et al.,
171 2011; Ding et al., 2011). PIN3 relocation in response to gravity in columella root cells is seen
172 in as little as 2 min, while the relocation of PIN7-GFP requires approximately 30 min to be
173 detected (Friml et al., 2002; Kleine-Vehn et al., 2010; Pernisova et al., 2016; Grones et al.,
174 2018). We examined plants harboring both *PIN7a-GFP* and *PIN7b-RFP* cDNAs under short
175 and long gravitropic stimuli. We did not find any difference in relocation dynamics between
176 both isoforms in these experiments (Supplemental Figures 3A-3D). We observed no
177 difference in the polarity change between PIN7a-GFP and PIN7b-RFP in hypocotyl
178 gravitropic (Rakusová et al., 2011; Rakusová et al., 2016) and phototropic (Ding et al., 2011)
179 bending assays (Supplemental Figures 3E-3I; due to limited transparency of hypocotyls, we
180 used lines expressing the cDNAs under strong endodermal *SCARECROW* (*SCR*) promoter
181 (Rakusová et al., 2011)). These data indicate that the different subcellular pathways driving
182 both PIN7a-GFP and PIN7b-RFP cargos are not connected with their ability to change
183 polarity in response to tropic stimuli.

184 Several studies employed the fluorescence recovery after photobleaching (FRAP)
185 analysis to investigate the dynamic turnover of various proteins, including PINs, on PM (Men
186 et al., 2008; Martinière et al., 2012; Langowski et al., 2016). We therefore bleached a region
187 of the PM signal in the root meristem of the *PIN7a-GFP* and *PIN7b-GFP* cDNA lines and
188 measured the FRAP in this area. Notably, PIN7a-GFP showed a slower recovery of
189 fluorescence than PIN7b-GFP (Figure 3A). The difference in the recovery speed and also in

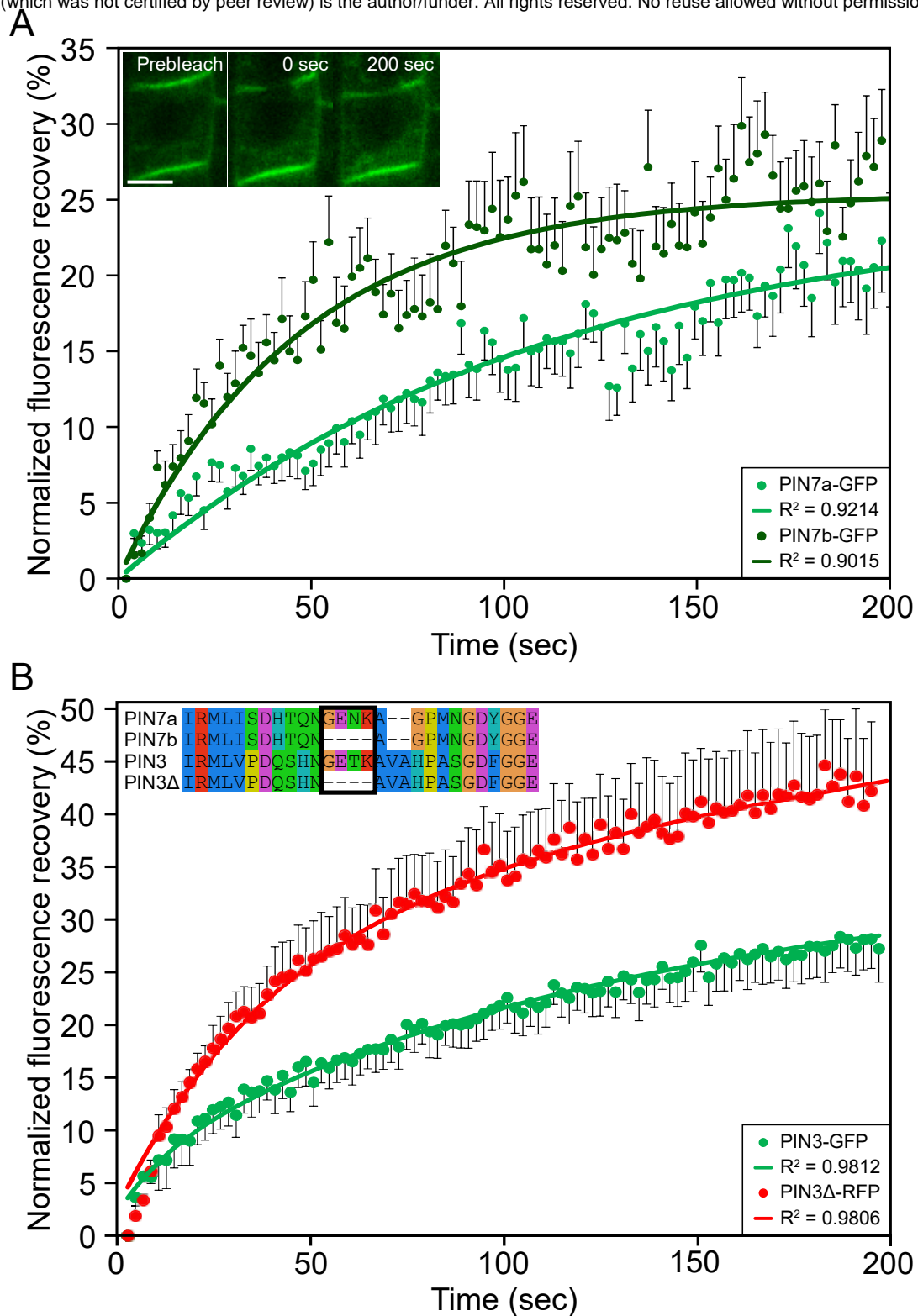


Figure 3. The cDNA encoded PIN7a and PIN7b isoforms tagged with fluorescent proteins show differential dynamics on the plasma membrane, as revealed by fluorescence recovery after photobleaching (FRAP).

(A) The PIN7a-GFP and PIN7b-GFP normalized FRAP, with single-phase exponential fitting curves. PIN7b-GFP shows different fluorescence recovery on the plasma membrane, compared to the longer PIN7a-GFP. The example image of the bleached region in cells is shown on the inset.

(B) The PIN3Δ-RFP and PIN3-GFP normalized FRAP, with single-phase exponential fitting curves. PIN3Δ-RFP, which lacks the 4 amino acid motif to mimic the properties of the PIN7b isoform, shows faster fluorescence recovery, in comparison to the control PIN3-GFP.

Bars, 5 μ m. Data are means, error bars are \pm S. E. At least 3 membranes in 5-6 root tips were analyzed in each experiment ($n \geq 20$).

See also Supplemental Figures 3 and 4.

190 the overall mobile phase ratio was even more pronounced when we used lines expressing both
191 cDNAs under the stronger *SCR* promoter (Supplemental Figure 4A); the choice of GFP or
192 RFP tag did not markedly interfere with the fluorescence recovery (Supplemental Figure 4B).
193 To validate our observations further, we generated plants carrying a *PIN3::PIN3Δ-RFP*
194 cDNA construct, which lacks the GETK motif corresponding to the four amino acids absent
195 in PIN7b (Figures 1B and 3B). The PIN3Δ-RFP signal showed an incomplete co-localization
196 with the wild type PIN3-GFP variant in the BFA bodies (Supplemental Figures 4C and 4D),
197 and faster recovery on the PM, analogous to that observed for PIN7a and PIN7b (Figure 3B).
198 It therefore appears that the motif altered by AS of PIN7 is required for the regulation of
199 dynamics of individual isoforms within the PM.

200

201 ***PIN7* splice isoforms are functionally different, based on the phenotype rescue tests**

202 To explore the role of the *PIN7* splice isoforms in plant development, we tested the
203 ability of their fluorescently tagged cDNAs to complement the phenotypes associated with the
204 *PIN7* locus. We initially selected the phototropic hypocotyl bending assay, which is highly
205 dependent on the activity of the PIN3 clade proteins (Friml et al., 2002; Willige et al., 2013).
206 We were unable to detect significant defects in the single *pin7-2* knockout (Friml et al., 2003)
207 itself, even at a detailed temporal resolution (Supplemental Figure 5A). As weak phenotypes
208 of the *pin7-2* loss of function mutants are the result of redundancy with other genes from the
209 *PIN3* clade (Friml et al., 2003; Blilou et al., 2005; Willige et al., 2013), we further employed a
210 triple *pin3-3 pin4-101 pin7-102* knock out (*pin347*) as a genetic background, which lacks the
211 phototropic response almost completely (Willige et al., 2013). Here, *PIN7a-GFP* cDNA was
212 able to rescue the phototropic bending, while the *PIN7b-RFP* cDNA did not show any effect,
213 regardless of whether the native (Figure 4A) or a strong endodermal *SCR* promoter
214 (Supplemental Figure 5B), was used. The choice of the tag does not appear to have any effect
215 in these assays, as evidenced by the lines where the fluorophore sequences have been
216 swapped (Figure 4B). Together, these data indicate that the motif changed by AS alters the
217 function of the PIN7 protein in *Arabidopsis*.

218 *PIN7a*, but not *PIN7b*, cDNA rescues the *pin347* phenotypes in the hypocotyl bending
219 test, and PIN3 clade auxin efflux carriers have been implicated in numerous instances of
220 auxin-mediated development. We therefore tested whether in some them the role of the
221 particular isoform could be prevalent. These processes include: determining of root
222 protoxylem formation (Bishopp et al., 2011) (Figure 4C), lateral root density (Swarup et al.,
223 2008) (Figure 4D), vertical direction of the root growth (Friml et al., 2002; Kleine-Vehn et al.,

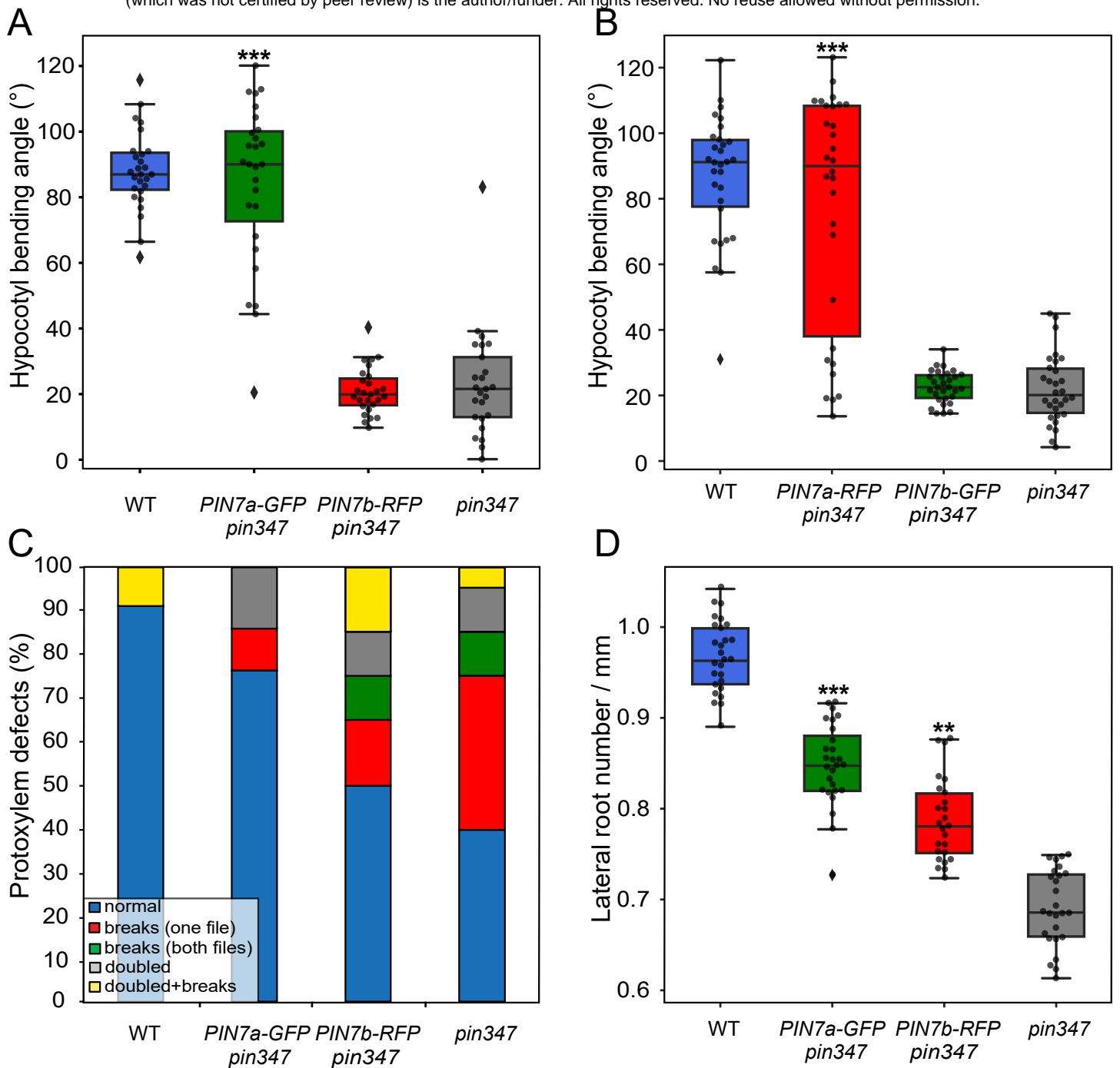


Figure 4. In contrast to PIN7b, the PIN7a cDNA under control of the natural PIN7 promoter complements phenotypes associated with the PIN7 locus.

(A) Phototropic bending of the etiolated *pin347* seedlings carrying the *PIN7a-GFP* and *PIN7b-RFP* constructs.

(B) Phototropic bending of the etiolated *pin347* seedlings carrying the *PIN7a-RFP* and *PIN7b-GFP* constructs.

(C and D) Quantification of the primary root protoxylem defects (C) and lateral root primordia (D) initiation of the *pin347* seedlings harboring the *PIN7a-RFP* and *PIN7b-GFP* constructs.

On (A), (B) and (D), the middle line corresponds to median, the box corresponds to the 25% and 75% quartiles, the whiskers correspond to minima and maxima, dots represent single data points. The asterisks indicate significance between respective line and the *pin347* mutant control (** $P < 0.01$, *** $P < 0.001$ by ANOVA). For each line in each experiment, at least 15 seedlings were analyzed ($n \geq 15$).

See also Supplemental Figure 5.

224 2010; Pernisova et al., 2016) (Supplemental Figure 5C), lateral root orthogravitropism
225 (Rosquete et al., 2013) (Supplemental Figure 5D), gravity-induced hypocotyl bending
226 (Rakusová et al., 2011) (Supplemental Figure 5E), number of rosette branches after
227 decapitation (Bennett et al., 2016) (Supplemental Figure 5F) and the overall rosette size
228 (Bennett et al., 2016) (Supplemental Figure 5G). Similar to the results above, the *PIN7a-GFP*
229 cDNA usually almost completely rescued the tested phenotypes, while the contribution of
230 *PIN7b-RFP* was smaller or even undetectable. This suggests that the functional roles of both
231 isoforms are common, regardless of the phenotype observed.

232

233 **A fluorescent reporter for studying the *PIN7a* and *b* expression**

234 The levels of *PIN7* (and *PIN4*) AS transcripts seem to be at comparable levels in most
235 organs (Figure 1C and Supplemental Figure 1A). However, this may not describe the actual
236 situation at the resolution of individual cells. To address this, we designed a dual fluorescent
237 reporter, which allows for monitoring the activity of the AS of *PIN7* *in planta* and *in situ*
238 (Figure 5A). Indeed, in the primary root or in the hypocotyl, we observed generally
239 overlapping expression of both isoforms without any obvious tissue preference (Figure 5B;
240 Supplemental Figure 6A). However, there were several instances in the vegetative tissue,
241 where the ratio of reporter signals appears to be uneven. These include early lateral root
242 primordia (Figure 5C), the mature pericycle adjacent to the phloem area (Supplemental Figure
243 6B), the stomatal lineage ground cells of the cotyledons (Supplemental Figure 6C), and the
244 concave side of opening apical hook (Figures 5D), where the *PIN7b-RFP* signal prevailed
245 over that of *PIN7a-GFP*. In general, these data corroborate the presence of both isoforms in
246 most cells and suggest that they may function in a coordinated manner.

247

248 **The combined activity of both *PIN7a* and *PIN7b* is required for apical hook formation** 249 **and tropic responses**

250 The occasional exaggerated response of the *pin347* mutants containing the *PIN7a-*
251 *GFP* transgene (Supplemental Figure 5E) prompted us to re-design phenotypic tests and adapt
252 our experimental methodology to carefully record the temporal dynamics of the processes
253 linked with the PIN3 clade function. We turned to apical hook development where the time
254 scale measurements of the PIN-mediated development have been well established (Zadnikova
255 et al., 2010). We also analyzed *pin4-101 pin7-102 (pin34)* mutants and a newly generated
256 *pin347* line that carried a combination of both *PIN7* cDNA constructs. Similar to gravi- and
257 phototropic experiments, the *PIN7b-RFP* cDNA generally did not complement the severe

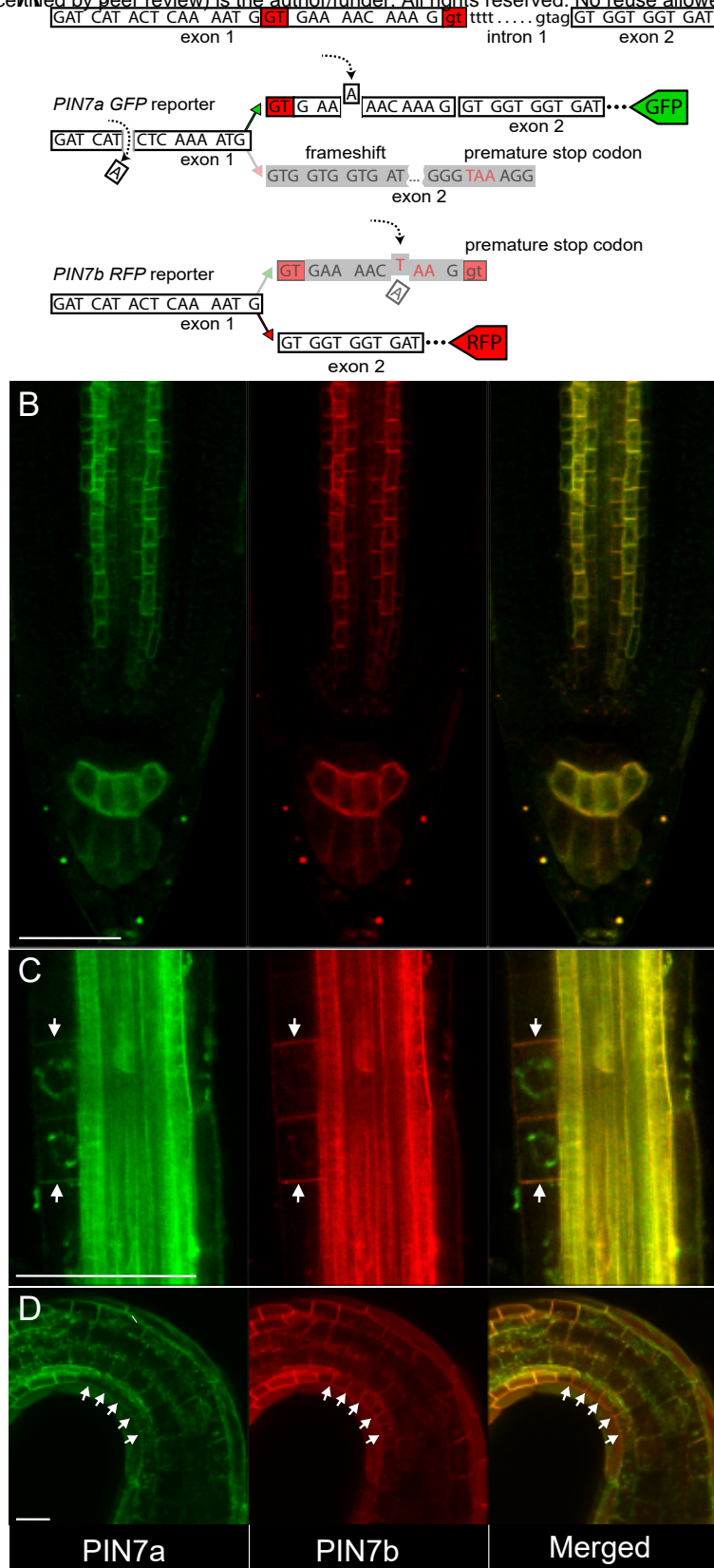


Figure 5. Reporter-based expression analysis of PIN7a and PIN7b isoforms across tissues.

(A) A scheme of the PIN7 splicing reporter. The reporter consists of two constructs: the PIN7a-GFP part contains two point mutations (marked with dashed arrows) and leads to the frameshift and its subsequent restoration when the PIN7a transcript is solely produced. PIN7b-RFP reporter carries a premature stop codon inside the protruding PIN7a region (dashed arrow below).

(B) PIN7a-GFP and PIN7b-RFP expression overlap in the root tip.

(C and D) PIN7b-RFP expression (arrows) PIN7a-GFP in the early lateral root primordia (C) and in the epidermis on the concave side of apical hook (D). The green signal in the perinuclear region of the lateral root primordia is an autofluorescence artifact.

For each tissue, at least 10 plants were analyzed ($n \geq 10$). Bars, 50 μm .

See also Supplemental Figure 6.

258 *pin347* phenotype. Expression of the *PIN7a-GFP* cDNA in *pin347* indeed led to partial rescue
259 of the apical hook formation defects, even surpassing the values observed for *pin34*.
260 Surprisingly, the simultaneous expression of both *PIN7a-GFP* and *PIN7b-RFP* suppressed the
261 dominant effects conferred by the *PIN7a-GFP* cDNA alone and phenocopied the *pin34*
262 mutant (Figure 6A; this effect was not caused by suppressing the expression of *PIN7a-GFP* by
263 the other transgene, Supplemental Figure 6D). This strongly suggests that both isoforms act in
264 a mutually opposing manner to modulate the processes of apical hook development.

265 Apical hook formation is a complex process that involves several bending steps
266 (Zadnikova et al., 2010), and the splicing reporter suggests a slightly different expression
267 pattern of *PIN7a* and *b* isoforms during apical hook development (Figure 5D). The hypocotyl
268 phototropic and gravity response includes only a single bending (Rakusová et al., 2011;
269 Rakusová et al., 2016), and the expression of the reporter appears to be uniform in the
270 respective tissue (Supplemental Figure 6A). Tracking dynamic bending of hypocotyls can
271 thus provide a hint to whether one can account for the antagonistic behavior of both isoforms
272 to differential expression or to their different dynamics during subcellular trafficking or at the
273 PM. Similar to apical hook development (Figure 6A), introducing the *PIN7b-RFP* cDNA did
274 not have any effect on the *pin347* phenotype, while the expression of *PIN7a-GFP* lead to
275 more rapid bending than that observed for the *pin34* mutant. Finally, the presence of both
276 *PIN7a-GFP* and *PIN7b-RFP* cDNAs in *pin347* was reminiscent of the *pin34* phenotype in
277 both phototropic and gravity assays (Figures 6B and 6C). We therefore conclude that the
278 shared activity of both PIN7 isoforms, likely conferred by their different trafficking or PM
279 retention properties, but probably not by their differential expression, is required for proper
280 apical hook formation and auxin-mediated tropic responses.

281

282 **DISCUSSION**

283 In this study, we show that AS diversifies the portfolio of PIN proteins present in
284 *Arabidopsis thaliana*. At the cellular level, AS does not alter the ability of the PIN7 proteins
285 to transport auxin *per se* or their overall subcellular localization, but it changes their dynamics
286 on the PM. In general, AS modifies protein properties variably. It can affect protein
287 subcellular localization, ligand binding affinity, enzymatic or transporting activities, protein
288 stability or the presence of covalent post-translational modifications (Stamm et al., 2005;
289 Kelemen et al., 2013). Different covalent modifications alter the subcellular trafficking of
290 most PINs. Phosphorylation sites on serine, threonine or tyrosine residues of various PINs
291 have been identified; their phosphorylation status also changes PIN-mediated tropic responses

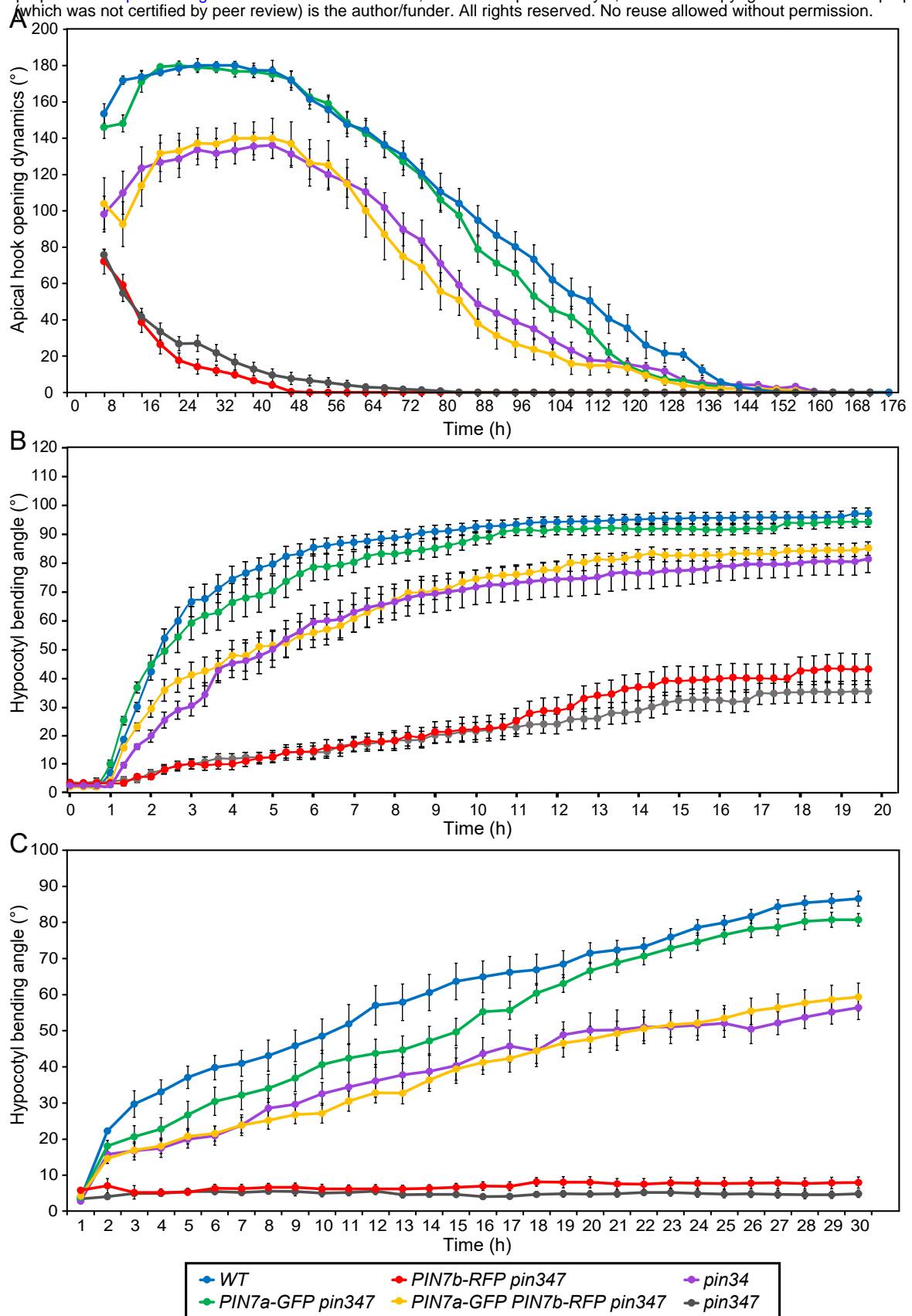


Figure 6. The simultaneous presence of PIN7a-GFP and PIN7b-RFP cDNA constructs in *pin347* phenocopies the *pin34* knock out mutant during apical hook opening and hypocotyl gravitropic bending.

(A-C) Temporal dynamics of etiolated *pin347* seedlings carrying the PIN7a-GFP and PIN7b-RFP transgenes examined (A) during apical hook development, (B) hypocotyl phototropic and (C) gravitropic bending.

Data are means \pm S. E. For each data point, the values obtained from 15 vertically grown seedlings were assessed (n = 15).

292 (Rademacher and Offringa, 2012; Barbosa et al., 2018; Zwiewka et al., 2019). Also PIN
293 ubiquitination (on lysines) and controlled proteolytic degradation act in auxin-mediated
294 processes (Leitner et al., 2012). However, none of the candidate residues required for these
295 modifications is present in the vicinity of the amino acid motif changed by AS. This region,
296 present inside the PIN long hydrophilic loop shows low amino acid conservation and it is
297 perhaps intrinsically disordered (Figure 1C) (Zwiewka et al., 2019). One can therefore
298 speculate whether it may change, perhaps by its length, the ability to assemble internal PIN
299 domains within the long hydrophilic group (Buljan et al., 2013) and modulate their interaction
300 affinity with other factors required for the entry and presence in secretory pathways and/or for
301 PIN7 dynamics at the PM.

302 We also present genetic evidence that the mutual activity of PIN7a and PIN7b is
303 operational during apical hook formation and tropic responses. We also tested major
304 functional aspects linked with the cellular activity of PIN7 that might be responsible for the
305 observed phenotypes (Adamowski and Friml, 2015). We found the differences between
306 PIN7a and PIN7b at the level of the PM recycling pathways and the stability on the plasma
307 membrane. It was previously demonstrated that the dynamics of PINs on the PM is controlled
308 in principle by two factors: by lateral diffusion in earlier phases and by dynamic recycling
309 from the secretory pathways in longer timelines (Kleine-Vehn et al., 2008a; Kleine-Vehn et
310 al., 2011; Langowski et al., 2016). As the effect of secretion or recycling has been evidenced
311 to be minor within 10 min after photobleaching (Kleine-Vehn et al., 2011; Langowski et al.,
312 2016), it seems that lateral diffusion significantly participates on the differential behavior of
313 PIN7a and PIN7b. In accordance with previous findings (Kleine-Vehn et al., 2011; Feraru et
314 al., 2011; Langowski et al., 2016), slower PIN7a FRAP rates suggest that PIN7 properly
315 functions when only associated with a larger complex or inside stable membrane clusters.
316 According to the earlier published model (Langowski et al., 2016), it therefore seems that
317 PIN7b probably antagonizes PIN7a action by impeding the polar auxin flow provided by
318 PIN7a in these membrane domains (Supplemental Figure 6E).

319 The mutually antagonistic interaction between two splice isoforms (or a similar
320 coordinated mechanism) has generally been already proposed in *Arabidopsis* (Szakonyi and
321 Duque, 2018). The seed dormancy regulator *DELAY OF GERMINATION 1 (DOG1)* is
322 processed into five mRNAs. Only the expression of two or more DOG1 cDNAs under the
323 native promoter rescues the *dog1* phenotype by synergistic stabilization of the protein by its
324 multimerization (Nakabayashi et al., 2015). The transcriptional factor HYH (HY5
325 HOMOLOG) possesses an isoform, which lacks a domain required for proteasomal

326 degradation, which leads to its increased stability and probably works as a semi-dominant
327 splice variant (Sibout et al., 2006; Szakonyi and Duque, 2018). The example of AS of PIN7 is
328 thus one of the first instances in plants where the mutually antagonistic effects of two splice
329 isoforms are observed on a single gene.

330

331 **EXPERIMENTAL PROCEDURES**

332 **Plant material and plant growth conditions**

333 All plant material, except tobacco cell cultures, was in the *Arabidopsis thaliana* (L.)
334 Heynh., Col-0 ecotype. These mutant and transgenic lines were described previously:
335 *PIN3::PIN3-GFP* (Zadnikova et al., 2010), *PIN4::PIN4-GFP*, *PIN7::PIN7-GFP* (Blilou et
336 al., 2005), *pin3-3 pin4-101 pin7-102 (pin347)*, *pin3-3 pin4-101 (pin34)* (Willige et al., 2013),
337 *pin7-2* (Friml et al., 2003).

338 For the *in vitro* cultivation, the seeds were surface-sterilized for 5 h with chlorine gas,
339 plated on 0.5× Murashige & Skoog medium with 1 % sucrose, and then stratified for 2 d at
340 4°C in darkness. Unless indicated otherwise, the seedlings were grown on vertically oriented
341 plates for 4-6 days under 16 h : 8 h photoperiod, 22 : 18°C, light : dark.

342 The following chemicals were used for treatments: brefeldin A (BFA), cytochalasin D
343 (CytD), oryzalin (Ory), β-estradiol, 2,4-dichlorophenoxyacetic acid (2,4-D), all from Sigma
344 (Sigma-Aldrich, St. Louis, MO, USA). Radioactively labeled auxin accumulation assays were
345 performed with [³H]NAA (naphthalene-1-acetic acid; 20 Ci.mmol⁻¹; American Radiolabeled
346 Chemicals, St. Louis, MO, USA).

347

348 **DNA manipulations and transgenic work**

349 The genomic *PIN7::PIN7-RFP* construct was made by replacing the GFP coding
350 sequence in the original *PIN7::PIN7-GFP* construct (Blilou et al., 2005). For creating the
351 *PIN7(4)::PIN7(4)a-GFP* and *PIN7(4)::PIN7(4)b-RFP* cDNA constructs, the respective
352 cDNAs were cloned into the pDONR221 P5-P2 entry vector (Invitrogen, Life Technologies,
353 Carlsbad, CA., USA) by the Gateway BP reaction (Invitrogen). The *Xba*I restriction site was
354 introduced at the 1350 bp (for *PIN7*) or 1341 bp (for *PIN4*) position of the cDNA coding
355 region for placing the fluorophore tag sequence. In parallel, the *PIN7* (or *PIN4*) promoters
356 were inserted into the pH7WG Gateway vector (Department of Plant Systems Biology, Ghent
357 University, Belgium; Karimi et al., 2002) by the Gibson Assembly kit (New England Biolabs,
358 Ipswich, MA, USA). The tagged *PIN7* and *PIN4* cDNA entry clones were then recombined
359 with the modified pH7WG destination vector by the Gateway LR reaction (Invitrogen). For

360 the cloning of the *PIN7* splicing dual fluorescent reporter, the entry vectors carrying the
361 genomic sequence of *PIN7-GFP* and *PIN7-RFP* (Adamowski and Friml, 2015), respectively,
362 were modified by inverse PCR. The resulting constructs were then recombined by the
363 Gateway LR reaction with the *PIN7* promoter containing the pH7WG destination vector. The
364 *SCR::PIN7a-GFP* and *SCR::PIN7b-RFP* constructs were obtained by recombination of the
365 *SCR* promoter in pDONR221 P1-P5r and *PIN7* cDNA entry clones with the pH7WG
366 destination vector by the Multisite Gateway LR reaction. *PIN3Δ-RFP* cDNA was custom
367 synthesized (Gen9, Ginkgo Bioworks, Boston, MA, USA), cloned into pDONR221 P5-P2
368 vector and together with the *PIN3* promoter pDONR221 P1-P5r construct recombined into the
369 pH7WG vector with Multisite Gateway. The validated binary constructs were transformed
370 into *Arabidopsis* by floral dipping. For making the estradiol-inducible *G10-*
371 *90::XVE>>AtPIN7(4)a-GFP*, and *G10-90::XVE>>AtPIN7(4)b-GFP* constructs, tagged *PIN7*
372 or *PIN4* cDNA entry clones were recombined with the pMDC7 destination vector (Curtis and
373 Grossniklaus, 2003) by the Gateway LR reaction. Unless stated otherwise, the constructs
374 present in the study were cloned under their natural *PIN4* or *PIN7* promoter. Primers used in
375 this work are listed in Supplemental Table 1.

376 For the generation of the stable transgenic lines carrying the cDNA constructs, at least
377 eight independent descendant populations of primary transformants were preselected for the
378 presence of the fluorescent signal. The functional validity of the cDNA constructs was
379 verified in the phototropic bending test, where all candidate lines matched the presented
380 results. Selected lines were used for further phenotypic analysis.

381

382 **Plant phenotype analysis**

383 The dynamic seedling development was tracked in the custom made dynamic
384 morphogenesis observation chamber equipped with blue and white LED unilateral light
385 sources, infra-red LED back light and a camera for imaging in the infra-red spectra, controlled
386 by the Raspberry Pi3B microcomputer (Raspberry Pi foundation, Cambridge, UK). For the
387 hypocotyl bending assays, the plated seeds were first illuminated for 6 h with white light. The
388 plates were then transferred to the observation chamber for 3-4 d. For the hypocotyl
389 phototropic bending experiments (Friml et al., 2002), the dark-grown seedlings were
390 afterward illuminated for 20 h with unilateral white light and imaged every 20 minutes. For
391 hypocotyl gravitropic bending experiments (Rakusová et al., 2011), the dark-grown seedlings
392 were rotated by 90° clockwise and imaged for 30 h every 60 min. For tracking apical hook
393 development, the seeds were first illuminated for 6 h with white light. They were then

394 transferred to the observation chamber and their development recorded every 4 h for a total
395 150 - 200 h in infrared spectra. Germination time was set as time 0, when first traces of the
396 main root were observed, individually for each seedling analyzed. Apical hook was
397 determined as an angle between the immobile (non-bending) part of hypocotyl and the distal
398 edge of cotyledons (Zadnikova et al., 2010), using the ImageJ software (Rueden et al., 2017).
399 At least 15 seedlings were analyzed for each line. Each experiment was done at least three
400 times.

401 For protoxylem defects analysis, 5-d old light-grown seedlings were cleared and
402 analyzed as described previously (Bishopp et al., 2011). For examining lateral root density, 8-
403 d old light-grown seedlings were cleared and observed with a DIC microscope (Dubrovsky et
404 al., 2009). Lateral root density was calculated by dividing the total number of lateral roots and
405 lateral root primordia to the length of the main root as described (Dubrovsky et al., 2009).
406 Vertical Growth Index (VGI), defined as a ratio between main root ordinate and main root
407 length, was quantified on 5-d old seedlings as published previously (Grabov et al., 2005). For
408 measuring the Gravitropic Set-point Angle (GSA), plates with 14-d old light-grown seedlings
409 were scanned and the angles between the vertical axis and five innermost 0.5 mm parts of
410 lateral root were determined as described previously (Roychoudhry et al., 2017). In all cases,
411 12-20 seedlings were analyzed for each line. Each experiment was done at least three times.

412 For decapitation experiments, 4-week short-day grown plants were moved into long-
413 day conditions to induce flowering. After the primary bolt reached 10-15 cm, the plant was
414 decapitated. The number of rosette branches was recorded at 7, 10 and 14-d after decapitation
415 (Greb et al., 2003; Waldie and Leyser, 2018). Rosette size was inspected in 18-d light-grown
416 plants prior to documenting. 10 plants were analyzed for each line, the experiment was done
417 three times.

418

419 **Microscopy**

420 Bright-field microscopy (differential interference contrast, DIC) was conducted on the
421 Olympus BX61 instrument (Olympus, Shinjuku, Tokyo, Japan) equipped with a DP50 camera
422 (Olympus). Routine confocal microscopy was performed on inverted Zeiss Axio Observer.Z1
423 containing the standard confocal LSM880 and Airyscan modules with 20x/0.8 DIC M27 air,
424 40x/1.2 W Kor FCS M27 air and 63x/1.40 Oil DIC M27 objectives (Carl Zeiss AG, Jena,
425 Germany). Gravity-induced polarity change experiments were carried out on Zeiss Axio
426 Observer.Z1 with vertically oriented sample position and the 40x/0.75 glycerol objective.

427 To observe the light-induced polarity change of PIN7a-GFP and PIN7b-RFP, 4-d
428 dark-grown seedlings were irradiated for 4 h with unilateral white light and then imaged with
429 Zeiss Axio Observer.Z1 LSM880 with a vertically oriented sample position, as described
430 (Willige et al., 2013). For analyzing gravity-induced polarity change, 4-d dark-grown
431 seedlings were reoriented by 90° clockwise and imaged 6 and 24 h after rotation, as described
432 (Rakusová et al., 2011).

433 For BFA treatments, 5-d light-grown seedlings were transferred to liquid 0.5× MS
434 media containing 50 μM BFA. The membrane/cytosol ratio was determined with ImageJ, it
435 was defined as the mean membrane signal intensity divided by the mean fluorescence in the
436 cytosol. For cytoskeleton depolymerizing drug treatments (Geldner et al., 2001), 5-d light-
437 grown seedlings were transferred to liquid 0.5× MS media supplemented with 20 μM of
438 cytochalasin D or 20 μM oryzalin. The co-treatments were done by the direct addition of
439 BFA. For the BFA removal, prior to the addition of the cytoskeleton depolymerizing
440 compounds, seedlings were twice washed out with fresh media and then transferred to that
441 supplemented with the respective cytoskeleton-depolymerizing drug.

442

443 **Fluorescent recovery after photobleaching (FRAP)**

444 For the FRAP experiments, Zeiss Axio Observer.Z1 equipped with the LSM880
445 confocal and Airyscan modules and the 40x/1.2 W Kor FCS M27 air objective was used. A
446 rectangular region of interest (ROI) of 40 x 20 pixels was selected on the basal or apical PM
447 of cells inside the vascular cylinder in the primary root meristematic area of 5-d light-growth
448 seedlings. ROI was bleached with the maximum 488 nm laser intensity and fluorescence
449 recovery was documented every 1 or 2 sec for a total 200 sec. Recovery time lapses were
450 analyzed with ImageJ. The Slices Alignment plugin (Tseng et al., 2012) for ImageJ was used
451 for the elimination of cell movement caused by root growth. In parallel, another rectangular
452 ROI (100 x 20 pixels) on the non-bleached cell was selected as a reference. To compensate
453 for the fluorophore bleaching during the recovery period, the data were normalized using
454 equation (Laňková et al., 2016)

$$455 \quad I_n = \frac{\left(\frac{I_t}{I_{t_{ref}}}\right) - \left(\frac{I_{min}}{I_{min_{ref}}}\right)}{\left(\frac{I_{max}}{I_{max_{ref}}}\right) - \left(\frac{I_{min}}{I_{min_{ref}}}\right)},$$

456 where I_n is normalized fluorescence intensity, I_t is the intensity at the specific time point,
457 I_{max} is the intensity after the initial bleaching, I_{max} is the intensity before initial bleaching.
458 $I_{t_{ref}}$, $I_{max_{ref}}$ and $I_{min_{ref}}$ represent the same values for the reference ROI. At least 3 membranes

459 in 4-5 root tips were analyzed in each experiment. Single-phase exponential fitting was
460 applied to the normalized FRAP data (SigmaPlot, Systat Software, Chicago, ILL, US) as
461 described (Sprague and McNally, 2005; Laňková et al., 2016). Recovery half-time is defined
462 as a time required for the fluorescence recovery to reach half of the steady-state fluorescence
463 intensity (Soumpasis, 1983; Sprague and McNally, 2005).

464

465 **Tobacco cell lines and auxin accumulation assays**

466 Tobacco cell line BY-2 (*Nicotiana tabacum* L. cv. Bright Yellow 2) was cultivated as
467 described (Müller et al., 2019). BY-2 cells were transformed with the pMDC7 constructs by
468 co-cultivation with *Agrobacterium tumefaciens* strain GV2260 as earlier described (Petrasek
469 et al., 2006; Müller et al., 2019). The transgene expression was maintained by cultivation on
470 media supplemented with 40 $\mu\text{g}\cdot\text{ml}^{-1}$ hygromycin (Roche) and 100 $\mu\text{g}\cdot\text{ml}^{-1}$ cefotaxime
471 (Sigma). Accumulation assays of radioactively labeled auxin were performed as previously
472 published (Delbarre et al., 1996; Petrasek et al., 2006) with cells cultured for 2 days in β -
473 estradiol or DMSO mock treatments. Presented results are from 3 biological replicates for
474 each representative *PIN7a* and *PIN7b* line and were confirmed for each on two other
475 independent genotypes. Independent β -estradiol inductions were done within 3-9 months after
476 the establishment of the cell suspension on lines, which showed comparable levels of the
477 expressed PIN7-GFP signal.

478

479 **Statistics and sequence analysis**

480 For two groups mean comparison, Student's *t*-test was applied. Statistical analysis of
481 multiple groups was performed by one-way ANOVA with subsequent Tukey HSD post-hoc
482 test. All statistical tests, including normality tests, were performed in R-studio IDE (R-studio,
483 Boston, MA, USA). In the box plots, the whisker length was defined as $Q \pm 1.5 \times \text{IQR}$, where
484 Q is the corresponding quartile and IQR is the interquartile range. For creating the multiple
485 sequence alignments, the protein sequences were aligned using the Clustal Omega algorithm
486 (Sievers et al., 2011) and graphically outlined by Mega-X, using default ClustalX color code
487 (Kumar et al., 2018).

488

489 **ACKNOWLEDGMENT**

490 We thank Claus Schwechheimer for the *pin34* and *pin347* seeds, Huibin Han for
491 assistance with the hypocotyl imaging, Dmitry Konovalov for help with the evolutionary
492 analysis, Karel Müller for the initial qRT-PCR analyses of the tobacco cell lines and Ksenia

493 Timofeyenko and Jozef Mravec for discussions. This work was supported by the Czech
494 Science Foundation (16-26428S) to I. K., M. H. and K. R., and the Ministry of Education,
495 Youth and Sports of the Czech Republic (MEYS, CZ.02.1.01/0.0/0.0/16_019/0000738) to K.
496 R. Imaging Facility of the Institute of Experimental Botany is supported by MEYS (projects
497 LM2018129 - Czech BioImaging, ERDF CZ.02.1.01/0.0/0.0/16_013/0001775 and OPVK
498 CZ.2.16/3.1.00/21519).

499

500 AUTHOR CONTRIBUTIONS

501 I. K., M. H., R. F., Z. V., D. R., and J. P. conducted experiments. J. H. enabled making
502 part of this project in his laboratory. S. S. and J. F. provided unpublished material. I. K., J. P.,
503 T. B. J., M. J. F., J. F., J. P., and K. R. conceived the research and designed experiments. K.
504 R. and I. K. wrote the manuscript. All authors read and commented on the final version of the
505 manuscript.

506

507 DECLARATION OF INTERESTS

508 The authors declare no competing interests.

509

510 REFERENCES

511 **Adamowski, M., and Friml, J.** (2015). PIN-Dependent Auxin Transport: Action, Regulation,
512 and Evolution. *Plant Cell* **27**:20–32.

513 **Barbosa, I. C. R., Hammes, U. Z., and Schwechheimer, C.** (2018). Activation and Polarity
514 Control of PIN-FORMED Auxin Transporters by Phosphorylation. *Trends in Plant*
515 *Science* **23**:523–538.

516 **Bazin, J., Romero, N., Rigo, R., Charon, C., Blein, T., Ariel, F., and Crespi, M.** (2018).
517 Nuclear Speckle RNA Binding Proteins Remodel Alternative Splicing and the Non-
518 coding Arabidopsis Transcriptome to Regulate a Cross-Talk Between Auxin and
519 Immune Responses. *Front Plant Sci* **9**:1209.

520 **Bennett, T., Brockington, S. F., Rothfels, C., Graham, S. W., Stevenson, D., Kutchan, T.,**
521 **Rolf, M., Thomas, P., Wong, G. K.-S., Leyser, O., et al.** (2014). Paralogous
522 Radiations of PIN Proteins with Multiple Origins of Noncanonical PIN Structure. *Mol*
523 *Biol Evol* **31**:2042–2060.

524 **Bennett, T., Hines, G., Rongen, M. van, Waldie, T., Sawchuk, M. G., Scarpella, E.,**
525 **Ljung, K., and Leyser, O.** (2016). Connective Auxin Transport in the Shoot
526 Facilitates Communication between Shoot Apices. *PLOS Biology* **14**:e1002446.

527 **Bishopp, A., Help, H., El-Showk, S., Weijers, D., Scheres, B., Friml, J., Benková, E.,**
528 **Mähönen, A. P., and Helariutta, Y.** (2011). A mutually inhibitory interaction

- 529 between auxin and cytokinin specifies vascular pattern in roots. *Curr. Biol.* **21**:917–
530 926.
- 531 **Blencowe, B. J.** (2017). The Relationship between Alternative Splicing and Proteomic
532 Complexity. *Trends in Biochemical Sciences* **42**:407–408.
- 533 **Blilou, I., Xu, J., Wildwater, M., Willemsen, V., Paponov, I., Friml, J., Heidstra, R.,
534 Aida, M., Palme, K., and Scheres, B.** (2005). The PIN auxin efflux facilitator
535 network controls growth and patterning in Arabidopsis roots. *Nature* **433**:39–44.
- 536 **Boutté, Y., Crosnier, M.-T., Carraro, N., Traas, J., and Satiat-Jeunemaitre, B.** (2006).
537 The plasma membrane recycling pathway and cell polarity in plants: studies on PIN
538 proteins. *J. Cell. Sci.* **119**:1255–1265.
- 539 **Buljan, M., Chalancon, G., Dunker, A. K., Bateman, A., Balaji, S., Fuxreiter, M., and
540 Babu, M. M.** (2013). Alternative splicing of intrinsically disordered regions and
541 rewiring of protein interactions. *Current Opinion in Structural Biology* **23**:443–450.
- 542 **Casson, S. A., Topping, J. F., and Lindsey, K.** (2009). MERISTEM-DEFECTIVE, an RS
543 domain protein, is required for the correct meristem patterning and function in
544 Arabidopsis. *The Plant Journal* **57**:857–869.
- 545 **Cheng, C.-Y., Krishnakumar, V., Chan, A. P., Thibaud - Nissen, F., Schobel, S., and
546 Town, C. D.** (2017). Araport11: a complete reannotation of the Arabidopsis thaliana
547 reference genome. *The Plant Journal* **89**:789–804.
- 548 **Curtis, M. D., and Grossniklaus, U.** (2003). A gateway cloning vector set for high-
549 throughput functional analysis of genes in planta. *Plant Physiol.* **133**:462–469.
- 550 **Darracq, A., and Adams, K. L.** (2013). Features of evolutionarily conserved alternative
551 splicing events between Brassica and Arabidopsis. *New Phytologist* **199**:252–263.
- 552 **Delbarre, A., Muller, P., Imhoff, V., and Guern, J.** (1996). Comparison of mechanisms
553 controlling uptake and accumulation of 2,4-dichlorophenoxy acetic acid, naphthalene-
554 1-acetic acid, and indole-3-acetic acid in suspension-cultured tobacco cells. *Planta*
555 **198**:532–541.
- 556 **Ding, Z., Galván-Ampudia, C. S., Demarsy, E., Łangowski, Ł., Kleine-Vehn, J., Fan, Y.,
557 Morita, M. T., Tasaka, M., Fankhauser, C., Offringa, R., et al.** (2011). Light-
558 mediated polarization of the PIN3 auxin transporter for the phototropic response in
559 Arabidopsis. *Nat Cell Biol* **13**:447–452.
- 560 **Dubrovsky, J. G., Soukup, A., Napsucialy-Mendivil, S., Jeknic, Z., and Ivanchenko, M.
561 G.** (2009). The lateral root initiation index: an integrative measure of primordium
562 formation. *Ann. Bot.* **103**:807–817.
- 563 **Feraru, E., Feraru, M. I., Kleine-Vehn, J., Martinière, A., Mouille, G., Vanneste, S.,
564 Vernhettes, S., Runions, J., and Friml, J.** (2011). PIN Polarity Maintenance by the
565 Cell Wall in Arabidopsis. *Current Biology* **21**:338–343.

- 566 **Friml, J., Wiśniewska, J., Benková, E., Mendgen, K., and Palme, K.** (2002). Lateral
567 relocation of auxin efflux regulator PIN3 mediates tropism in Arabidopsis. *Nature*
568 **415**:806–809.
- 569 **Friml, J., Vieten, A., Sauer, M., Weijers, D., Schwarz, H., Hamann, T., Offringa, R., and**
570 **Jürgens, G.** (2003). Efflux-dependent auxin gradients establish the apical-basal axis
571 of Arabidopsis. *Nature* **426**:147–153.
- 572 **Ganguly, A., Park, M., Kesawat, M. S., and Cho, H.-T.** (2014). Functional Analysis of the
573 Hydrophilic Loop in Intracellular Trafficking of Arabidopsis PIN-FORMED Proteins.
574 *Plant Cell* **26**:1570–1585.
- 575 **Geldner, N., Friml, J., Stierhof, Y. D., Jürgens, G., and Palme, K.** (2001). Auxin transport
576 inhibitors block PIN1 cycling and vesicle trafficking. *Nature* **413**:425–428.
- 577 **Ghelli, R., Brunetti, P., Napoli, N., Paolis, A. D., Cecchetti, V., Tsuge, T., Serino, G.,**
578 **Matsui, M., Mele, G., Rinaldi, G., et al.** (2018). A Newly Identified Flower-Specific
579 Splice Variant of AUXIN RESPONSE FACTOR8 Regulates Stamen Elongation and
580 Endothecium Lignification in Arabidopsis. *Plant Cell* **30**:620–637.
- 581 **Glanc, M., Fendrych, M., and Friml, J.** (2018). Mechanistic framework for cell-intrinsic re-
582 establishment of PIN2 polarity after cell division. *Nat. Plants* **4**:1082–1088.
- 583 **Grabov, A., Ashley, M. K., Rigas, S., Hatzopoulos, P., Dolan, L., and Vicente-Agullo, F.**
584 (2005). Morphometric analysis of root shape. *New Phytol.* **165**:641–651.
- 585 **Greb, T., Clarenz, O., Schafer, E., Muller, D., Herrero, R., Schmitz, G., and Theres, K.**
586 (2003). Molecular analysis of the LATERAL SUPPRESSOR gene in Arabidopsis
587 reveals a conserved control mechanism for axillary meristem formation. *Genes Dev.*
588 **17**:1175–1187.
- 589 **Grones, P., Abas, M., Hajný, J., Jones, A., Waidmann, S., Kleine-Vehn, J., and Friml, J.**
590 (2018). PID/WAG-mediated phosphorylation of the Arabidopsis PIN3 auxin
591 transporter mediates polarity switches during gravitropism. *Sci Rep* **8**:10279.
- 592 **Hrtyan, M., Šliková, E., Hejátko, J., and Růžička, K.** (2015). RNA processing in auxin and
593 cytokinin pathways. *J. Exp. Bot.* **66**:4897–4912.
- 594 **Kalyna, M., Lopato, S., and Barta, A.** (2003). Ectopic Expression of atRSZ33 Reveals Its
595 Function in Splicing and Causes Pleiotropic Changes in Development. *Mol. Biol. Cell*
596 **14**:3565–3577.
- 597 **Karimi, M., Inzé, D., and Depicker, A.** (2002). GATEWAYTM vectors for Agrobacterium-
598 mediated plant transformation. *Trends in Plant Science* **7**:193–195.
- 599 **Kelemen, O., Convertini, P., Zhang, Z., Wen, Y., Shen, M., Falaleeva, M., and Stamm, S.**
600 (2013). Function of alternative splicing. *Gene* **514**:1–30.
- 601 **Keren, H., Lev-Maor, G., and Ast, G.** (2010). Alternative splicing and evolution:
602 diversification, exon definition and function. *Nat Rev Genet* **11**:345–355.

- 603 **Kleine-Vehn, J., Dhonukshe, P., Sauer, M., Brewer, P. B., Wiśniewska, J., Paciorek, T.,**
604 **Benková, E., and Friml, J. (2008a).** ARF GEF-Dependent Transcytosis and Polar
605 Delivery of PIN Auxin Carriers in Arabidopsis. *Current Biology* **18**:526–531.
- 606 **Kleine-Vehn, J., Langowski, Ł., Wiśniewska, J., Dhonukshe, P., Brewer, P. B., and**
607 **Friml, J. (2008b).** Cellular and Molecular Requirements for Polar PIN Targeting and
608 Transcytosis in Plants. *Molecular Plant* **1**:1056–1066.
- 609 **Kleine-Vehn, J., Ding, Z., Jones, A. R., Tasaka, M., Morita, M. T., and Friml, J. (2010).**
610 Gravity-induced PIN transcytosis for polarization of auxin fluxes in gravity-sensing
611 root cells. *PNAS* **107**:22344–22349.
- 612 **Kleine-Vehn, J., Wabnik, K., Martinière, A., Langowski, Ł., Willig, K., Naramoto, S.,**
613 **Leitner, J., Tanaka, H., Jakobs, S., Robert, S., et al. (2011).** Recycling, clustering,
614 and endocytosis jointly maintain PIN auxin carrier polarity at the plasma membrane.
615 *Molecular Systems Biology* **7**:540.
- 616 **Klepikova, A. V., Kasianov, A. S., Gerasimov, E. S., Logacheva, M. D., and Penin, A. A.**
617 (2016). A high resolution map of the Arabidopsis thaliana developmental
618 transcriptome based on RNA-seq profiling. *Plant J.* **88**:1058–1070.
- 619 **Kriechbaumer, V., Wang, P., Hawes, C., and Abell, B. M. (2012).** Alternative splicing of
620 the auxin biosynthesis gene YUCCA4 determines its subcellular compartmentation.
621 *Plant J.* **70**:292–302.
- 622 **Kumar, S., Stecher, G., Li, M., Knyaz, C., and Tamura, K. (2018).** MEGA X: Molecular
623 Evolutionary Genetics Analysis across Computing Platforms. *Molecular Biology and*
624 *Evolution* **35**:1547–1549.
- 625 **Langowski, L., Wabnik, K., Li, H., Vanneste, S., Naramoto, S., Tanaka, H., and Friml, J.**
626 (2016). Cellular mechanisms for cargo delivery and polarity maintenance at different
627 polar domains in plant cells. *Cell Discov* **2**:16018.
- 628 **Laňková, M., Humpolíčková, J., Vosolobě, S., Cit, Z., Lacek, J., Čovan, M., Čovanová,**
629 **M., Hof, M., and Petrášek, J. (2016).** Determination of Dynamics of Plant Plasma
630 Membrane Proteins with Fluorescence Recovery and Raster Image Correlation
631 Spectroscopy. *Microscopy and Microanalysis* **22**:290–299.
- 632 **Leitner, J., Petrášek, J., Tomanov, K., Retzer, K., Pařezová, M., Korbei, B., Bachmair,**
633 **A., Zažímalová, E., and Luschnig, C. (2012).** Lysine63-linked ubiquitylation of
634 PIN2 auxin carrier protein governs hormonally controlled adaptation of Arabidopsis
635 root growth. *PNAS* **109**:8322–8327.
- 636 **Li, H.-T., Yi, T.-S., Gao, L.-M., Ma, P.-F., Zhang, T., Yang, J.-B., Gitzendanner, M. A.,**
637 **Fritsch, P. W., Cai, J., Luo, Y., et al. (2019).** Origin of angiosperms and the puzzle
638 of the Jurassic gap. *Nat. Plants* **5**:461–470.
- 639 **Marquez, Y., Brown, J. W. S., Simpson, C., Barta, A., and Kalyna, M. (2012).**
640 Transcriptome survey reveals increased complexity of the alternative splicing
641 landscape in Arabidopsis. *Genome Res.* **22**:1184–1195.

- 642 **Marquez, Y., Höpfler, M., Ayatollahi, Z., Barta, A., and Kalyna, M.** (2015). Unmasking
643 alternative splicing inside protein-coding exons defines exitrons and their role in
644 proteome plasticity. *Genome Res.* **25**:995–1007.
- 645 **Martinière, A., Lavagi, I., Nageswaran, G., Rolfe, D. J., Maneta-Peyret, L., Luu, D.-T.,**
646 **Botchway, S. W., Webb, S. E. D., Mongrand, S., Maurel, C., et al.** (2012). Cell
647 wall constrains lateral diffusion of plant plasma-membrane proteins. *PNAS*
648 **109**:12805–12810.
- 649 **Mei, W., Boatwright, L., Feng, G., Schnable, J. C., and Barbazuk, W. B.** (2017).
650 Evolutionarily Conserved Alternative Splicing Across Monocots. *Genetics* **207**:465–
651 480.
- 652 **Men, S., Boutté, Y., Ikeda, Y., Li, X., Palme, K., Stierhof, Y.-D., Hartmann, M.-A.,**
653 **Moritz, T., and Grebe, M.** (2008). Sterol-dependent endocytosis mediates post-
654 cytokinetic acquisition of PIN2 auxin efflux carrier polarity. *Nat. Cell Biol.* **10**:237–
655 244.
- 656 **Müller, K., Hošek, P., Laňková, M., Vosolobě, S., Malínská, K., Čarná, M., Filová, M.,**
657 **Dobrev, P. I., Helusová, M., Hoyerová, K., et al.** (2019). Transcription of specific
658 auxin efflux and influx carriers drives auxin homeostasis in tobacco cells. *Plant J.*
659 **100**:627–640.
- 660 **Nakabayashi, K., Bartsch, M., Ding, J., and Soppe, W. J. J.** (2015). Seed Dormancy in
661 Arabidopsis Requires Self-Binding Ability of DOG1 Protein and the Presence of
662 Multiple Isoforms Generated by Alternative Splicing. *PLOS Genetics* **11**:e1005737.
- 663 **Nodzyński, T., Vanneste, S., Zwiewka, M., Pernisová, M., Hejátko, J., and Friml, J.**
664 (2016). Enquiry into the Topology of Plasma Membrane-Localized PIN Auxin
665 Transport Components. *Molecular Plant* **9**:1504–1519.
- 666 **O’Leary, N. A., Wright, M. W., Brister, J. R., Ciufu, S., Haddad, D., McVeigh, R.,**
667 **Rajput, B., Robbertse, B., Smith-White, B., Ako-Adjei, D., et al.** (2016). Reference
668 sequence (RefSeq) database at NCBI: current status, taxonomic expansion, and
669 functional annotation. *Nucleic Acids Res.* **44**:D733-745.
- 670 **Pernisova, M., Prat, T., Grones, P., Harustiakova, D., Matonohova, M., Spichal, L.,**
671 **Nodzynski, T., Friml, J., and Hejatko, J.** (2016). Cytokinins influence root
672 gravitropism via differential regulation of auxin transporter expression and
673 localization in Arabidopsis. *New Phytologist* **212**:497–509.
- 674 **Petrasek, J., Mravec, J., Bouchard, R., Blakeslee, J. J., Abas, M., Seifertová, D.,**
675 **Wisniewska, J., Tadele, Z., Kubes, M., Covanová, M., et al.** (2006). PIN proteins
676 perform a rate-limiting function in cellular auxin efflux. *Science* **312**:914–918.
- 677 **Rademacher, E. H., and Offringa, R.** (2012). Evolutionary Adaptations of Plant AGC
678 Kinases: From Light Signaling to Cell Polarity Regulation. *Front. Plant Sci.* **3**.
- 679 **Rakusová, H., Gallego - Bartolomé, J., Vanstraelen, M., Robert, H. S., Alabadí, D.,**
680 **Blázquez, M. A., Benková, E., and Friml, J.** (2011). Polarization of PIN3-dependent
681 auxin transport for hypocotyl gravitropic response in Arabidopsis thaliana. *The Plant*
682 *Journal* **67**:817–826.

- 683 **Rakusová, H., Abbas, M., Han, H., Song, S., Robert, H. S., and Friml, J.** (2016).
684 Termination of Shoot Gravitropic Responses by Auxin Feedback on PIN3 Polarity.
685 *Current Biology* **26**:3026–3032.
- 686 **Reddy, A. S. N., Marquez, Y., Kalyna, M., and Barta, A.** (2013). Complexity of the
687 alternative splicing landscape in plants. *Plant Cell* **25**:3657–3683.
- 688 **Remy, E., Cabrito, T. R., Baster, P., Batista, R. A., Teixeira, M. C., Friml, J., Sá-
689 Correia, I., and Duque, P.** (2013). A major facilitator superfamily transporter plays a
690 dual role in polar auxin transport and drought stress tolerance in Arabidopsis. *Plant*
691 *Cell* **25**:901–926.
- 692 **Retzer, K., Butt, H., Korbei, B., and Luschig, C.** (2014). The far side of auxin signaling:
693 fundamental cellular activities and their contribution to a defined growth response in
694 plants. *Protoplasma* **251**:731–746.
- 695 **Rosquete, M. R., von Wangenheim, D., Marhavý, P., Barbez, E., Stelzer, E. H. K.,
696 Benková, E., Maizel, A., and Kleine-Vehn, J.** (2013). An Auxin Transport
697 Mechanism Restricts Positive Orthogravitropism in Lateral Roots. *Current Biology*
698 **23**:817–822.
- 699 **Roychoudhry, S., Kieffer, M., Del Bianco, M., Liao, C.-Y., Weijers, D., and Kepinski, S.**
700 (2017). The developmental and environmental regulation of gravitropic setpoint angle
701 in Arabidopsis and bean. *Sci Rep* **7**:42664.
- 702 **Rueden, C. T., Schindelin, J., Hiner, M. C., DeZonia, B. E., Walter, A. E., Arena, E. T.,
703 and Eliceiri, K. W.** (2017). ImageJ2: ImageJ for the next generation of scientific
704 image data. *BMC Bioinformatics* **18**:529.
- 705 **Ruzicka, K., Zhang, M., Campilho, A., Bodi, Z., Kashif, M., Saleh, M., Eeckhout, D., El-
706 Showk, S., Li, H., Zhong, S., et al.** (2017). Identification of Factors Required for
707 m6A mRNA Methylation in Arabidopsis Reveals a Role for the Conserved E3
708 Ubiquitin Ligase HAKAI. *New Phytol* **215**:157–172.
- 709 **Shang, X., Cao, Y., and Ma, L.** (2017). Alternative Splicing in Plant Genes: A Means of
710 Regulating the Environmental Fitness of Plants. *International Journal of Molecular*
711 *Sciences* **18**:432.
- 712 **Sibout, R., Sukumar, P., Hettiarachchi, C., Holm, M., Muday, G. K., and Hardtke, C. S.**
713 (2006). Opposite Root Growth Phenotypes of hy5 versus hy5 hyh Mutants Correlate
714 with Increased Constitutive Auxin Signaling. *PLOS Genetics* **2**:e202.
- 715 **Sievers, F., Wilm, A., Dineen, D., Gibson, T. J., Karplus, K., Li, W., Lopez, R.,
716 McWilliam, H., Remmert, M., Söding, J., et al.** (2011). Fast, scalable generation of
717 high - quality protein multiple sequence alignments using Clustal Omega. *Molecular*
718 *Systems Biology* **7**.
- 719 **Soumpasis, D. M.** (1983). Theoretical analysis of fluorescence photobleaching recovery
720 experiments. *Biophysical Journal* **41**:95–97.
- 721 **Sprague, B. L., and McNally, J. G.** (2005). FRAP analysis of binding: proper and fitting.
722 *Trends in Cell Biology* **15**:84–91.

- 723 **Staiger, D., and Brown, J. W. S.** (2013). Alternative splicing at the intersection of biological
724 timing, development, and stress responses. *Plant Cell* **25**:3640–3656.
- 725 **Stamm, S., Ben-Ari, S., Rafalska, I., Tang, Y., Zhang, Z., Toiber, D., Thanaraj, T. A.,**
726 **and Soreq, H.** (2005). Function of alternative splicing. *Gene* **344**:1–20.
- 727 **Swarup, K., Benková, E., Swarup, R., Casimiro, I., Péret, B., Yang, Y., Parry, G.,**
728 **Nielsen, E., De Smet, I., Vanneste, S., et al.** (2008). The auxin influx carrier LAX3
729 promotes lateral root emergence. *Nat. Cell Biol.* **10**:946–954.
- 730 **Szakonyi, D., and Duque, P.** (2018). Alternative Splicing as a Regulator of Early Plant
731 Development. *Front. Plant Sci.* **9**.
- 732 **Tress, M. L., Abascal, F., and Valencia, A.** (2017). Alternative Splicing May Not Be the
733 Key to Proteome Complexity. *Trends in Biochemical Sciences* **42**:98–110.
- 734 **Tseng, Q., Duchemin-Pelletier, E., Deshiere, A., Balland, M., Guillou, H., Filhol, O., and**
735 **Théry, M.** (2012). Spatial organization of the extracellular matrix regulates cell-cell
736 junction positioning. *Proc. Natl. Acad. Sci. U.S.A.* **109**:1506–1511.
- 737 **Tsugeki, R., Tanaka-Sato, N., Maruyama, N., Terada, S., Kojima, M., Sakakibara, H.,**
738 **and Okada, K.** (2015). CLUMSY VEIN, the Arabidopsis DEAH-box Prp16 ortholog,
739 is required for auxin-mediated development. *Plant J.* **81**:183–197.
- 740 **Waldie, T., and Leyser, O.** (2018). Cytokinin Targets Auxin Transport to Promote Shoot
741 Branching. *Plant Physiol.* **177**:803–818.
- 742 **Willige, B. C., Ahlers, S., Zourelidou, M., Barbosa, I. C. R., Demarsy, E., Trevisan, M.,**
743 **Davis, P. A., Roelfsema, M. R. G., Hangarter, R., Fankhauser, C., et al.** (2013).
744 D6PK AGCVIII Kinases Are Required for Auxin Transport and Phototropic
745 Hypocotyl Bending in Arabidopsis. *Plant Cell* **25**:1674–1688.
- 746 **Zadnikova, P., Petrášek, J., Marhavý, P., Raz, V., Vandenbussche, F., Ding, Z.,**
747 **Schwarzerová, K., Morita, M. T., Tasaka, M., Hejátko, J., et al.** (2010). Role of
748 PIN-mediated auxin efflux in apical hook development of Arabidopsis thaliana.
749 *Development* **137**:607–617.
- 750 **Zwiewka, M., Bilanovičová, V., Seifu, Y. W., and Nodzyński, T.** (2019). The Nuts and
751 Bolts of PIN Auxin Efflux Carriers. *Front Plant Sci* **10**.